energy&fuels

pubs.acs.org/EF

Process Modeling of an Innovative Power to LNG Demonstration Plant

Eduard Alexandru Morosanu,[†] Andrés Saldivia,[‡] Massimiliano Antonini,[‡] and Samir Bensaid*,[†]

[†]Department of Applied Science and Technology (DISAT), Politecnico di Torino, Corso Duca degli Abruzzi 24, 10129 Torino, Italy
[‡]HySyTech S.r.l., Strada del Drosso, 33/18, 10135 Torino, Italy

ABSTRACT: The continuous increase in electricity production from renewable energy sources (RESs) introduces the intrinsic fluctuating characteristic of RESs in the electric power grid, causing nontrivial grid management issues (e.g., grid congestion). In this work, an innovative power to liquefied methane concept was developed, and process simulations for a 200 kW_{el} demonstration plant were carried out. The proposed concept is based on water electrolysis to produce hydrogen, CO_2 capture from air using solid adsorption materials, catalytic CO_2 methanation, gas separation, and a single mixed refrigerant (SMR) liquefaction process. The gas separation unit produces an exhaust stream, rich in not only hydrogen and carbon dioxide but also methane, that is recycled to the methanation unit inlet. A thermodynamic analysis excluded the possibility of carbon deposition formation in the methanation reactor due to methane recirculation. The gas separation system was designed using a combination of temperature swing adsorption techniques (stream dehumidification) and membrane separation (CO_2 separation). After a screening of different polyimide-type membranes, a two-stage layout was selected and dimensioned. Subsequently the liquefaction unit was developed, optimizing the SMR composition and pressures to minimize the total work required. Hence, the minimum work required for the liquefaction resulted in being 0.57 kWh_{el}/kg_{LNG}. Finally, the thermal integration was performed to minimize the external heat requirement. The heat produced by the electrolyzer and methanation unit is greater than the thermal energy requirement by the CO_2 capturing unit during desorption. A process efficiency up to 46.3% (electric to chemical) resulted from the study. The process modeling results also evidenced that the impact of the gas pretreatment and liquefaction process on the plant energetics is 4% of the total power input.

1. INTRODUCTION

According to the Intergovernmental Panel on Climate Change (IPCC), human activity is responsible for climate change mainly due to the emission of greenhouse gases from fossil-fuel usage.[1] After the Kyoto protocol commitment, many climate change mitigation policies have been promulgated to reduce anthropogenic greenhouse gas emissions in the EU, and incentives were given to install renewable power plants (e.g., wind or solar) to reduce the dependency on fossil fuels.[2] Renewable energy sources (RESs) have a fluctuating and intermittent characteristic (daily or seasonal), with peak production generally not matching the demand.[3] As adoption of RESs grows in the electricity power source scenario, balancing of the electric grid without modulating the RES power plant is needed.

Different technologies are available and under study for this purpose: flywheels, supercapacitors, batteries,[4] compressed air storage,[5] pumped hydroelectric storage,[6] and power-to-fuels (gas[7] or liquid[8]). These solutions have been extensively reviewed in the literature along with their advantages and drawbacks.[9−12]

Power-to-gas (PtG) appears to be a promising solution in converting excess renewable electricity in an energy carrier. Water electrolysis is used to convert electricity into hydrogen, which, unfortunately, presents some drawbacks such as low-energy density, steel embrittlement, and challenges in storage/transportation. On the contrary, natural gas has a well-developed distribution grid and mature applications. Therefore, the most feasible solution is to further convert hydrogen in a substitute natural gas (SNG) compliant with the natural gas grid

specifications. SNG can be produced by mixing hydrogen with carbon dioxide to carry out the Sabatier reaction 1. This concept also has the advantage of recycling CO_2 and potentially preventing global warming.[13,14]

$$CO_2 + 4H_2 \rightleftharpoons CH_4 + 2H_2O \quad \Delta H_{298K} = -164.9 \text{ kJ/mol} \tag{1}$$
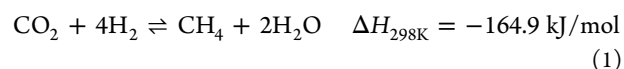
To implement this technology, three conditions must occur simultaneously: excess RES electricity, a carbon dioxide source (e.g., biogas upgrading to biomethane), and a nearby injection point for the product SNG. If a reliable carbon dioxide source is not available, then CO_2 sequestration from air might be a viable solution,[15] whereas if an injection point is not feasible, then liquefaction of the produced gas through a cryogenic process may be considered (Figure 1). On this last point, liquefying the produced gas would allow us to obtain a substitute liquefied natural gas.

In the past several years, liquid natural gas (LNG) has received much interest as new applications are being studied and developed in not only the niche application of natural gas transportation but also in:

- Heavy trucks and light-duty freight/passenger vehicles through the L-CNG filling stations concept providing both LNG to trucks and compressed natural gas (CNG) to light vehicles[16,17]
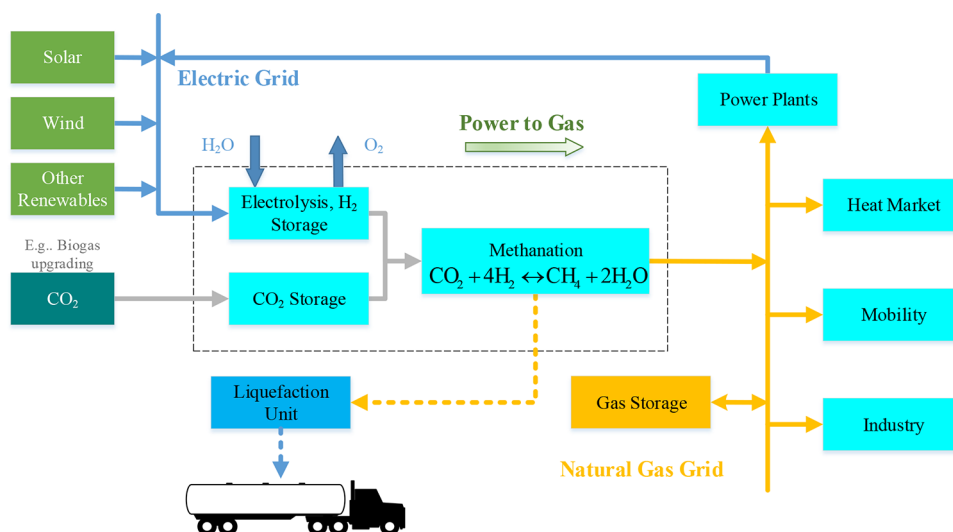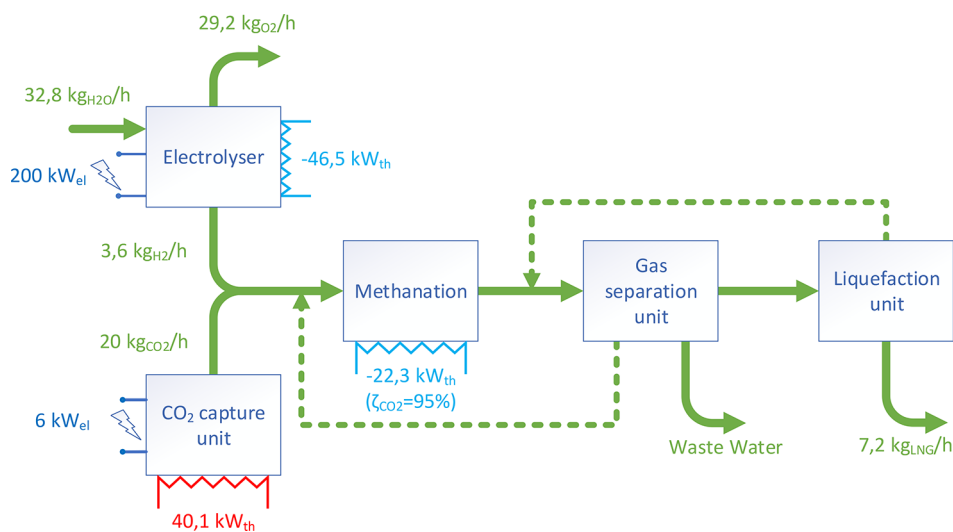
Figure 1. Power to Gas/LNG concept.

Figure 2. Block flow diagram with preliminary mass and energy balance.

- Marine transportation: By substituting diesel powered cargoes with LNG, a reduction of 90% of SO_x, 35% NO_x, 29% CO_2, and 85% carbon particulate is achievable[18,19]
- Fertilizer industry[20]
- Electricity production[20]

PtG has received much interest from the scientific community and industry. The first large-scale 6 MW_{el} PtG plant was built in Werlte (Germany) in the Audi e-gas project. The plant uses three alkaline water electrolyzers of 2 MW each and isothermal fixed-bed methanation reactors fed with CO_2 from a nearby biogas plant. The heat generated by the PtG plant is recovered in the biogas plant.[21,22] Another project called HelmetH built a demo plant using high-temperature steam electrolysis. The aim of the project is to demonstrate the high efficiency achievable by coupling the endothermic electrolysis to the exothermic methanation.[23] At least 25 demo projects using CO_2 methanation are reported in the literature.[22] However, in none of the 25 demos is liquefaction of the produced gas performed. A PtG process using this solution can be deployed in remote areas (e.g., islands), regions not covered by the natural gas distribution grid and off-grid applications.

In this Article, we focus on the process simulation of a novel demo plant that uses CO_2 captured from air and produces liquefied gas equivalent to LNG. The plant is being built in Troia, Italy, where a high quantity of wind and solar electricity is produced. This demo is one of the three plants that produce SNG and are being built in the EU cofunded Store&GO project framework.[24] The other two plants are being built in Falkenhagen, Germany and Solothurn, Switzerland.

2. PROCESS DESCRIPTION AND SIMULATION MODEL OVERVIEW

The demo plant is being built on the site of a previous project, called INGRID,[25] aimed at demonstrating the usage of solid hydrogen-storage systems for electric grid balancing. From this project the electrolyzer module was inherited. Also, other constraints on the operation conditions were present and are going to be discussed in the following subsections.

Hydrogen is produced through a water electrolyzer using renewable electricity. The produced hydrogen is then mixed with carbon dioxide captured from air. The reagents are mixed with the recycle stream, and the H_2-to-CO_2 ratio is maintained equal to the stoichiometric value of 4. Because the methanation
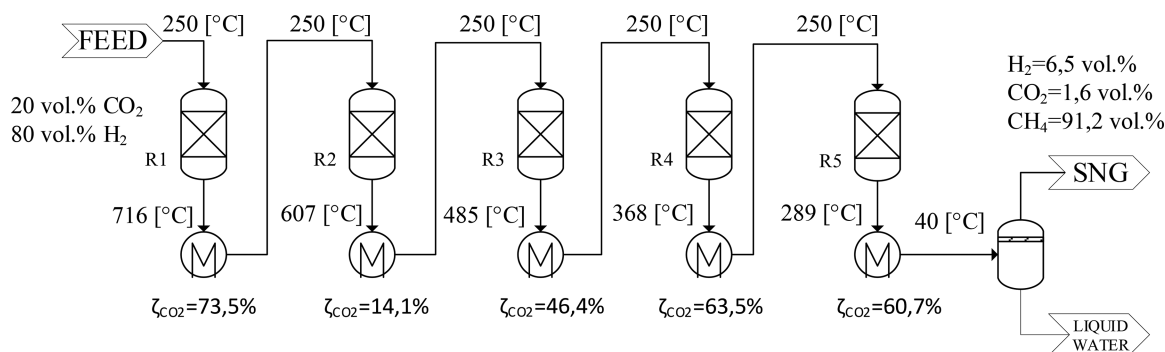
Figure 3. Series of five adiabatic reactors with intercooling operating at 10 bar.
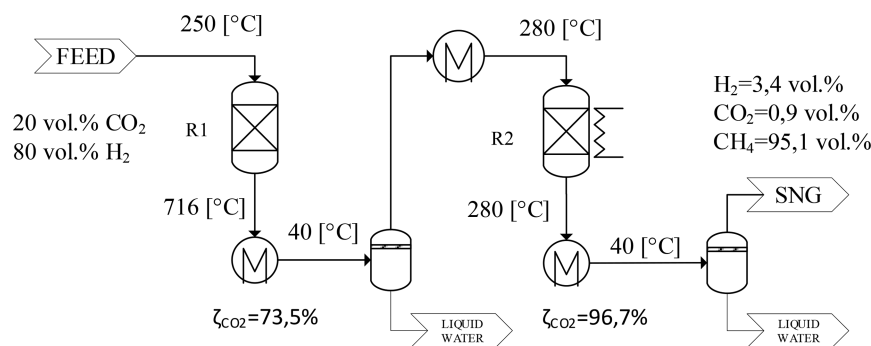

Figure 4. Series of an adiabatic and an isothermal reactor with intercooling and water condensation operating at 10 bar.

reaction is highly exothermic, the reactor must have adequate cooling to maintain as much isothermal operation as possible. After the methanation step, the stream is mainly made of water, methane, hydrogen, and carbon dioxide. Steam and carbon dioxide must be below a certain concentration to avoid freezing in the condenser during the liquefaction process. Therefore, the first operation after the methanation reactor is cooling the outlet stream to near-ambient temperature to remove most of the water content, then followed by a temperature swing adsorption (TSA) that further dries the stream. Subsequently, carbon dioxide is separated by using a membrane gas separation system, and the permeate (rich in carbon dioxide and hydrogen) is recycled to the methanation unit. A final TSA polishing unit brings the concentration of CO_2 to the required specification. The last step is the liquefaction of the synthetic gas obtaining LNG and a boil-off stream that is then recycled to the process. In Figure 2 the block flow diagram of the process is reported with preliminary mass and energy balance.

2.1. Electrolyser Unit. Different technologies of electrolyzers can be used to split water into hydrogen and oxygen: alkaline electrolysis cells (AECs), proton exchange membrane electrolysis cells (PEMECs), and solid oxide electrolysis cells (SOECs). The AECs and PEMECs are fed with liquid water and operate at low temperature (<200 °C), whereas in SOECs, steam electrolysis occurs at high temperature (700−900 °C). The most mature and low capital cost electrolysis technology is the AEC,[26] but it is generally characterized by comparatively lower efficiencies than SOEC and PEMEC. This is also the technology of the electrolyzer inherited from the INGRID project.

The AEC unit used in the demo has a power consumption of 4.9 kWh/Nm$^3_{H2}$ (AC power including all the utilities), and this translates to a module efficiency of 71.7% HHV basis (60.7% LHV basis). These units generally work between 50 and 80 °C

and can deliver high-purity hydrogen up to 15 barg without additional compression. The electrolyzer module of the demo plant can be fed with up to 200 kW of electricity. This allowed for the evaluation of the hydrogen flow rate and heat production.

2.2. CO$_2$ Capture Unit. The most common technology for CO_2 capture is based on gas scrubbing with amine solvents (e.g., monoethanolamine). This process is generally used in natural gas sweetening and biogas upgrading to biomethane. However, these processes have a high cost and energy consumption. Another solution under study is to use ionic liquids as an absorbent for the CO_2. This should overcome some negative aspects of the amine base processes (i.e., volatility, corrosion, and degradation).[27,28] However, these two solutions are generally used with streams with a considerable amount of carbon dioxide (e.g., flue gas). To capture CO_2 from air, where the mean concentration value is 400 ppm, one of the best solutions is to use an adsorption material. Therefore, by moving air through the adsorption material, carbon dioxide is captured. This process recovers the trapped carbon dioxide from the material using a desorption cycle (i.e., heating the material). The sorption material is generally functionalized with amine groups for a better selectivity toward carbon dioxide.[15,29−32] This is also the technology used in the demo plant. The specific energy requirements for the CO_2 capture unit were taken from the datasheet of a commercially available collector, and these are as follows: 200−300 kW$_{el}$/ton$_{CO_2}$ and 1500−2000 kWh$_{th}$/ton$_{CO_2}$ at 100 °C.[33] For the unit energetic requirements calculation, the worst-case scenario of 300 kW$_{el}$/ton$_{CO_2}$ and 2000 kWh$_{th}$/ton$_{CO_2}$ was used in the simulation.

2.3. CO$_2$ Methanation Unit. One of the Store&GO project aims is to demonstrate three different CO_2 methanation processes: modular milli-structured catalytic methanation reactors, catalytic honeycomb/structured wall methanation reactors, and biological methanation. The investigated demo
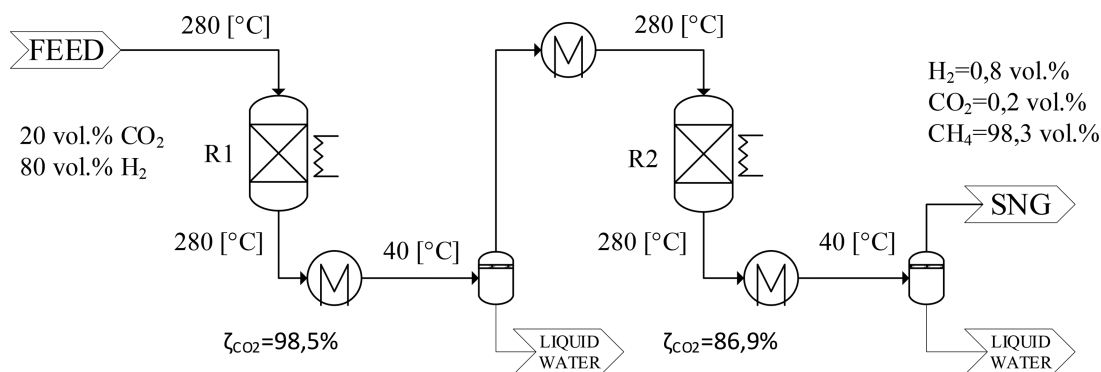
Figure 5. Series of two isothermal reactors with intercooling and water condensation operating at 10 bar.

can operate up to 10 bar with the methanation reactor for two main reasons: Hydrogen is produced up to 15 bar and an additional compressor will not be available; the milli-structure methanation reactor is built to withstand pressures up to 10 bar. Different reactor configurations that operate at 10 bar were considered:

(a) A series of five adiabatic reactors with intercooling: The equilibrium conversion 96% is reached at the outlet of the last reactor. The conversion was calculated using eq 2. In Figure 3, the layout of the five adiabatic reactors is reported along with further details of conversions and temperatures.

(b) Adiabatic and isothermal (operating at 280 °C) in series with intercooling and water condensation at 40 °C: This configuration reaches a conversion of 99.1%. The layout is represented in Figure 4. The temperature at the outlet of the first reactor is >700 °C, which is not compatible with most methanation catalysts. This is also a problem for the first configuration.

(c) Two isothermal reactors operating at 280 °C in series with intercooling and water condensation at 40 °C reaching 99.8% of conversion (Figure 5).

$$\zeta_{CO_2} = 1 - \frac{\dot{n}_{CO_2,out}}{\dot{n}_{CO_2,in}} \tag{2}$$

Even with the highest conversion achievable in the last case, the product gas does not meet the liquefaction specifications (see Section 2.4): A gas separation system is therefore needed. A single isothermal methanation reactor configuration for the methanation module was chosen because with this configuration a high conversion is possible and a purification step will be needed anyway. The reactor operates isothermally at 280 °C and at a total pressure between 4 and 10 bar. The pressure at which the reactor operates can vary to compensate the slow catalyst activity decay that may occur during the lifespan of the plant. This will also be object of investigation of the demo. From tests performed on a milli-structured reactor prototype, a set of operating conditions have been identified (not reported here) that guarantee a CO_2 conversion of 95% at 4 bar. The reactor was simulated as an yield reactor using this last value of conversion.

One of the deactivation phenomena that may occur during methanation is solid carbon formation on the catalyst surface, blocking the active sites of the catalyst by fouling. A thermodynamic analysis over a large range of compositions was performed to predict whether solid carbon formation can occur. Carbon deposition boundaries were identified in

representative temperature (250−650 °C) and pressure (4−10 bar) ranges that may be encountered in the methanation process.

The species that are involved in the reaction system are generally CO_2, H_2, CH_4, H_2O, CO, and solid carbon. In the range of operating conditions considered in this work, higher-molecular-mass hydrocarbons that may be formed are in the parts per million range and were neglected. The effect of neglecting these components was quantified by Tevebaugh et al.[34] In the worst case scenario the deviation in the results is ∼1%. According to Frick et al.,[35] under the considered operating conditions, the most likely species of carbon to be formed is graphitic carbon. Therefore, only graphitic carbon was considered in the calculations. The analysis was carried out by calculating the chemical equilibrium of the system using the Gibbs free-energy minimization method. The thermodynamic data were obtained from the National Institute of Standards and Technology (NIST),[36] while the simulations were carried out using the optimization toolbox present in MATLAB.

2.4. Gas Conditioning. The liquefaction unit typically requires the feed to have a carbon dioxide content lower than 50 ppm by volume (ppm_v) and a water concentration lower than 1 ppm by weight (ppm_w) to prevent freezing during liquefaction. Hydrogen, on the contrary, should not pose a problem. A gas-conditioning unit is therefore required. The first purification step is to remove water vapor generated by the reaction. The stream exits the reactor at 280 °C and is cooled to 40 °C, removing most of the water content by condensation. The remaining water vapor is removed through a TSA module. The next step is the removal of excess CO_2 for which different technologies are available: water scrubbing, pressure swing adsorption,[32] membrane gas separation,[37,38] temperature swing adsorption, and chemical scrubbing. In this case, a membrane gas separation system was used. The dehumidified stream must be compressed to 13 bar because membrane separation uses pressure difference as driving force. The membrane separation was simulated by using a shortcut design model for a hollow fiber module in counter-current operation.[39] This allowed the dimensioning of the module in terms of active area and the evaluation of the resulting streams in terms of flow rate and composition. Furthermore, a TSA was used as a polishing module to reach the required CO_2 concentration before entering the liquefaction unit.

2.5. Liquefaction Unit. Mainly three different technologies are available for natural gas liquefaction: cascade, expansion, and mixed refrigerant liquefaction processes.[40] The single mixed refrigerant (SMR) liquefaction process seems to be the best choice for small-scale liquefaction due its high efficiency and low
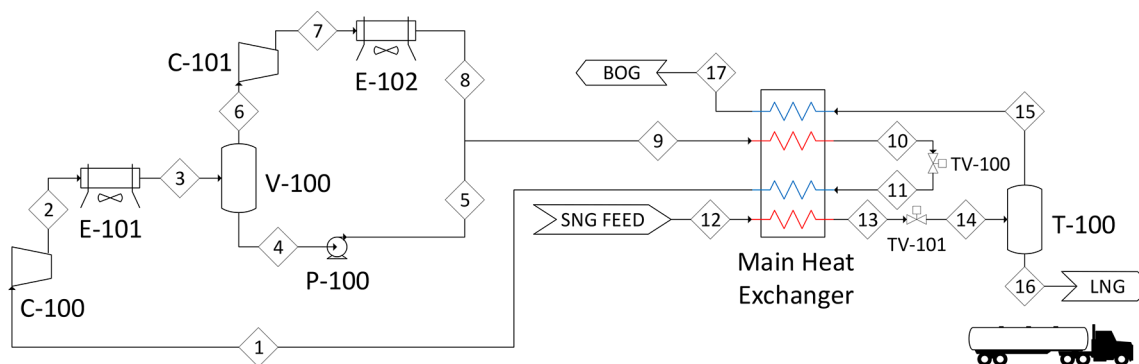
Figure 6. Flow diagram of the SMR process.

Table 1. Tested Membranes' Single Gas Permeability and Ideal Selectivity

	permeability (barrer)[a]			ideal selectivity	
	H_2	CO_2	CH_4	H_2/CH_4	CO_2/CH_4
M1. cellulose acetate[54]	2.6	9	0.43	6.2	21.1
M2. TBDA1-6FDA-PI[55]	253	155	3.3	76.7	46.9
M3. 6FDA-durene[56]	600	455.8	28.4	21.1	16.1
M4. TR-PBI (450)[57]	1779	1624	35	50.8	46.4

[a]1 barrer = $1 \times 10^{-10} \ cm^3_{STD} \ cm \ s^{-1} \ cm^{-2} \ cm^{-1}_{Hg}$

complexity (i.e., low number of equipment) compared with the other technologies.[41] Hence, this process was selected for the simulation of the liquefaction unit.

The considered SMR system is represented in Figure 6. The proposed system has a two-stage refrigerant compression section with interstage cooling. In the first stage the compressed refrigerant is cooled through an air-cooler (E-101) from which a biphasic stream could form. Therefore, a phase separator between the compression stages is present (V-100), followed by a pump (P-100) to transfer the condensate toward the main heat exchanger. Also, the outlet of the second compressor is cooled by an air-cooler (E-102), causing the vapor present in the stream to partially condensate. The resulting compressed refrigerant is then sent to the main heat exchanger, where it undergoes full condensation at −160 °C, followed by an isenthalpic lamination (TV-100). The stream then is used as the main coolant of the process. At this point the SNG is also fed to the main heat exchanger, where it is cooled and condensed at −160 °C. The obtained liquid SNG is laminated to the storage pressure of 2 bar. This allows for the evaluation of the boil-off gas (BOG) stream. Heat recovery is performed before recycling the BOG stream to the process.

An SMR process uses a mixture of nitrogen and hydrocarbons (C1 to C5) as refrigerant. The composition of the refrigerant has been tuned to follow the same trend as the hot composite curve, thus minimizing the required compression work on the refrigerant. The total work required for compression (represented by the sum of the duty of C-100, P-100, and C-101) was chosen as the objective function to be optimized. This function depends on the following parameters: refrigerant composition, condensation, and evaporation pressure. The optimization of the SMR process involves a nonlinear and strongly coupled system of equations: A robust optimization method is thus required. Different procedures to solve the optimization problem are present in literature: the box method, the graphical targeting approach, the genetic algorithm (GA), and derivative-free.[42] In this case, the GA was used and implemented according to Cao et al.[43]

For the simulation of this section, the following assumptions were made:

- No pressure drops in the heat exchangers and phase separators
- Refrigerant temperature at main Heat exchanger inlet of 40 °C
- Minimum temperature approach between cold and hot streams equal to 3 °C[43,44]
- Null cold box heat leakage
- Compressor adiabatic efficiency of 75%
- Refrigerant is a mixture of nitrogen, methane, ethane or ethylene, propane or propene, and isopentane

3. RESULTS AND DISCUSSION

3.1. Model Results. The target for the demo plant in terms of electricity to the electrolyzer was set equal to 200 kW, resulting in a total hydrogen production of 3.6 kg_{H_2}/h (41.3 N $m^3_{H_2}$/h). The CO_2 inlet flow was calculated by keeping the stoichiometric ratio (H_2/CO_2 = 4), including also the nonstoichiometric recycle stream. A CO_2 flow rate of 20 kg_{CO_2}/h (10.3 N $m^3_{CO_2}$/h) resulted from the simulation. The carbon dioxide capturing unit energy requirements are 6.0 kW of electricity and 40.1 kW of heat. Furthermore, the unit produces CO_2 at near-atmospheric pressure, requiring compression to the process pressure of 4 bar, meaning that an additional compressor is need whose power requirement was estimated in 0.8 kW of electricity (isentropic efficiency 75%). The methanation reactor feed is obtained by mixing the fresh H_2 and CO_2 streams with the recycle stream. The resulting feed stream is heated to 280 °C and the calculated duty of the heat exchanger is 5.3 kW. Because the reactor works in isothermal mode, the 21.9 kW of heat produced by the methanation reaction is removed. About 60% of the methanation outlet stream is made of water vapor, the majority of which (97.8%) is separated in an air-cooled condenser that cools the stream to 40 °C, resulting in a duty of the condenser of 14.8 kW. To reach the required specification

of <1 ppm$_w$ of H$_2$O for the liquefaction, the stream was further desiccated by using a TSA.

The dried stream is then compressed to 13 bar and sent to the membrane gas separation system, and the compressor duty at full capacity is 2.8 kW. Different types of membranes are available for CO$_2$ separation from natural gas like streams: polymeric, zeolite, carbon molecular sieves, and so on. The most used membrane type in CO$_2$ gas separation is the glassy polymer category thanks to their selectivity, excellent thin-film formation, good mechanical properties, and higher permeability to low-molecular-weight species.[45] In Table 1 the most interesting membranes that were used to perform the simulations are reported.

None of these membranes can reach the required gas purification in one stage of separation. In fact, the cut ratio of the module would be higher than 0.5, creating high recirculation flow rates with a high content of methane. Therefore, a two-stage system was developed where the permeate from the first module is recirculated to the methanation reactor inlet and the retentate stream is sent to the second module. From the second module, the permeate stream is compressed and sent back to the first stage inlet (Figure 7). With this arrangement, the specification
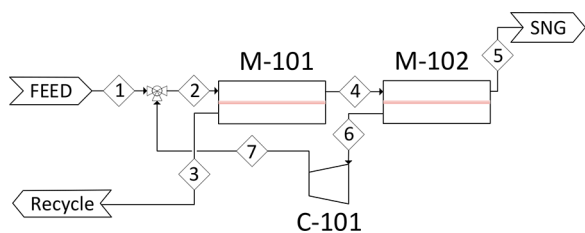

Figure 7. Membrane separation module.

<0.6% of CO$_2$ is met with two modules of 20 m^2 of active surface area, each made of membrane M2 (commercially available modules with equal performance). The cut ratio of membrane separation unit is 0.197, giving a recirculation stream to the methanation unit of 1.8 kg/h. Also, H$_2$ is separated, reducing the overall boil-off from the liquefaction stage and mass flow to the unit.

The retentate from the second membrane stage is sent to a TSA polishing unit that lowers the CO$_2$ content to <50 ppm$_v$. The resulting stream is ready to undergo the liquefaction process.

The optimization of the mixed refrigerant composition and pressures was carried out for the four refrigerant compositions. In Table 2, the optimization results are reported. The mole fractions for the low-temperature components (N$_2$ and CH$_4$) and high-temperature components (isopentane) do not change in a sensible manner between refrigerants. The main component in all of the mixtures is methane around 41%. The optimum lamination and compression outlet pressures do not change significantly. The lowest specific energy consumption was found

for the ethylene−propane containing refrigerants (0.57 kWh/kg$_{LNG}$). However, it is noteworthy that all of the refrigerant compositions are suitable for the liquefaction of SNG, with low differences in energy consumption under the assumed conditions (maximum 0.6 kWh/kg$_{LNG}$). Literature results of SMR systems used to liquefy natural gas show specific power consumptions lower than the ones found in this application (0.29 to 0.42 kWh/kg$_{LNG}$[40,43,44]). This difference could be attributed to the difference in composition. In this case, the gas that is being liquefied is basically pure methane. On the contrary, natural gas is not made of pure methane: 87−97% methane, 1.5−9% ethane, 0.2−5% nitrogen, and 0.1−1.5% propane.[46]

In Figure 8, the composite curves and the temperature difference between the hot and cold side are reported. The plots are relative to the optimized mixtures shown in Table 2. In all four mixtures the temperature difference curves have two main peaks. The right peak at high temperature is caused by a phase change in the cold stream, which is converted from liquid to vapor that has a lower heat capacity than the liquid. The left peak at low temperature is caused by a phase change in the hot stream, which is converted from vapor to liquid that has a higher heat capacity. Two pinch points are present in all four cases: one at low temperature (145 K, when the liquefaction of the SNG stream starts) and one at high temperature (313 K). The refrigerant that better glides the cold composite to the hot composite curve is the ethylene−propane, giving a lower mean temperature difference causing the slightly lower energy requirement. However, a lower average temperature difference also means that a greater heat-exchange area might be required, translating to a cost increase.

Two different scenarios arise in the management of the recycle streams: (a) recirculation of the membrane first-stage permeate and the boil-off stream directly to the methanation reactor and (b) recirculation of the boil-off with the second-stage membrane permeate to the membrane inlet compressor.

With the second arrangement, the recirculation of a methane-rich and high-flow-rate stream to the methanation reactor inlet is avoided, lowering the possibility of carbon deposition, whereas the composition of the membrane feed is marginally altered.
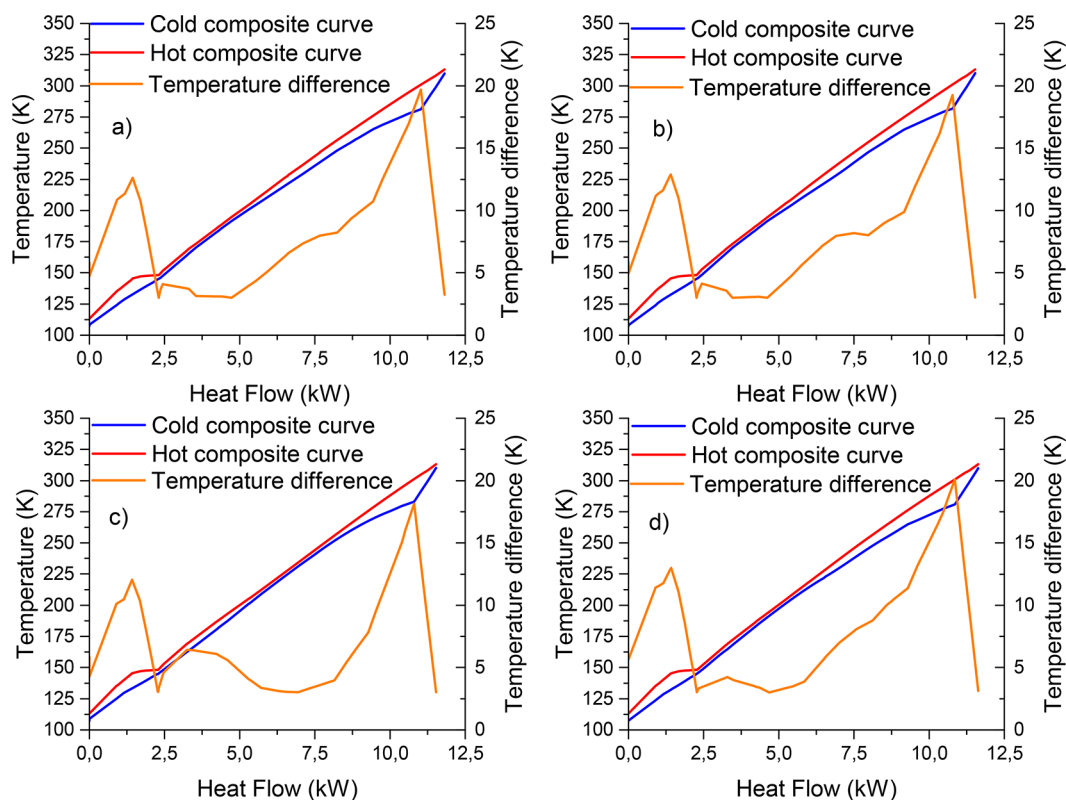
In Figure 9, the complete process flowsheet diagram is reported, and in Table 3, the associated stream table is reported.

3.2. C−H−O Diagrams with Carbon Deposition Boundaries. The results of the computations are represented by means of C−H−O ternary diagrams for an easy and immediate interpretation.

In Figure 10, the evaluation of the methane recirculation influence on the position of the operating condition on the ternary plot is shown. By increasing the methane content and maintaining the H$_2$/CO$_2$ ratio equal to 4, the operating condition moves on the line connecting the stoichiometric feed to pure methane. The intersection of this line with the carbon formation boundary isotherm gives the maximum

Table 2. Refrigerant Composition, Pressures, and Performance

	refrigerant composition (mol %)										
	N$_2$	CH$_4$	C$_2$H$_6$	C$_2$H$_4$	C$_3$H$_8$	C$_3$H$_6$	iso-pentane	P_{11} (bar)	P_9 (bar)	refrigerant flow (kg$_{REF}$/kg$_{LNG}$)	required work (kWh/kg$_{LNG}$)
1	13.0	41.3	18.5			13.1	14.0	3.2	33.4	7.9	0.59
2	12.6	41.6	19.1		13.1		13.7	3.2	32.1	8.0	0.59
3	12.0	42.1		17.9	13.7		14.3	3.4	32.6	7.9	0.57
4	13.9	39.6		14.5		18.8	13.2	3.3	33.3	8.1	0.60

Figure 8. Composite temperature curves and temperature difference for the optimized refrigerant composition (a) ethane−propane, (b) ethane−propene, (c) ethylene−propane, and (d) ethylene−propene.
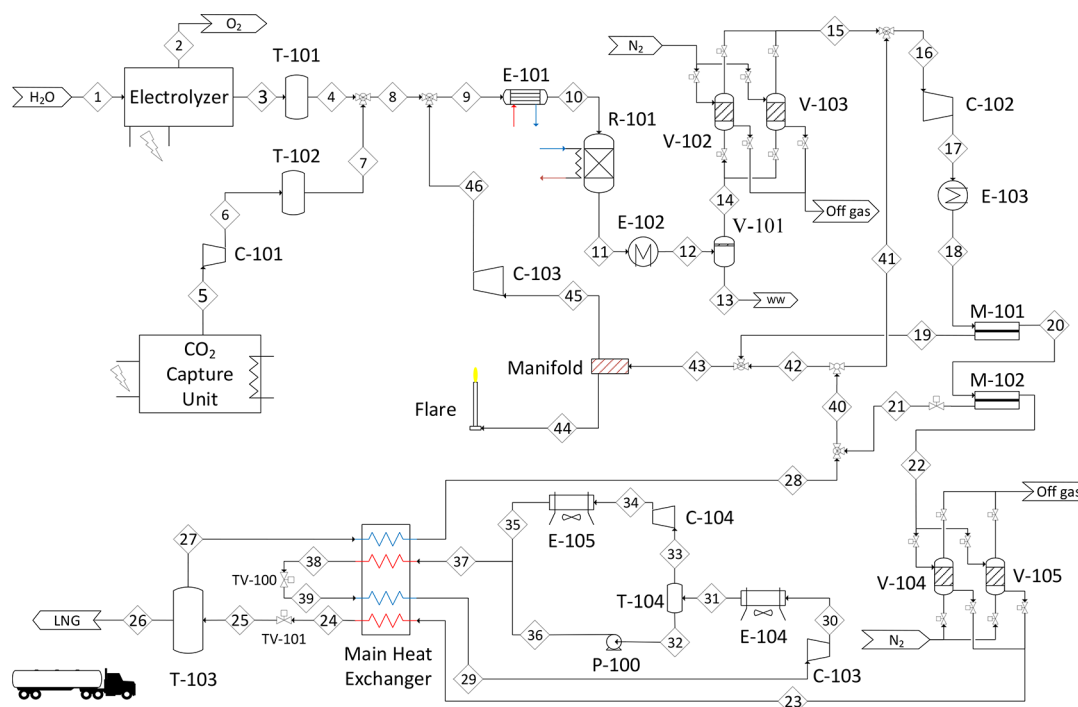
Figure 9. Process flow diagram.

methane concentration in the feed, after which carbon deposition is thermodynamically favored.

If the methane concentration is high enough to risk carbon formation, then water vapor can be added to the stream. This will move the operating point toward the stoichiometric

condition, where carbon formation is unfavorable, at least from a thermodynamic point of view (Figure 10).

The C−H−O ternary plots for 4, 6, 8, and 10 bar of total pressure are shown in Figure 11. It can be observed that the carbon deposition boundaries are little sensitive to pressure variations in the range that was analyzed. Three operating

Table 3. Stream Table of the Process Recycle Scheme A (Omitted Null or Least Important Streams)

|	mole fraction (mol %)				total flow				
	CO_2	CH_4	H_2	H_2O	(kmol/h)	(kg/h)	temperature (°C)	pressure (bar)	vapor fraction
1	0.0	0.0	0.0	100.0	1.81	32.6	75.0	15.0	0.00
4	0.0	0.0	100.0	0.0	1.81	3.6	20.0	5.0	1.00
5	100.0	0.0	0.0	0.0	0.45	20.0	20.0	1.0	1.00
7	100.0	0.0	0.0	0.0	0.45	20.0	20.0	5.0	1.00
9	19.6	1.8	78.6	0.0	2.42	25.5	20.6	5.0	1.00
10	19.6	1.8	78.6	0.0	2.42	25.5	260.0	4.0	1.00
11	1.6	32.6	6.3	59.5	1.52	25.5	280.0	2.0	1.00
12	1.6	32.6	6.3	59.5	1.52	25.5	40.0	2.0	0.42
14	3.7	78.1	15.0	3.2	0.63	9.5	40.0	2.0	1.00
15	3.9	80.6	15.5	0.0	0.61	9.2	40.0	2.0	1.00
16	4.0	78.4	17.6	0.0	0.70	10.3	38.7	1.2	1.00
18	4.0	78.4	17.6	0.0	0.70	10.3	35.0	13.2	1.00
19	13.2	27.4	59.4	0.0	0.16	1.8	35.0	1.2	1.00
20	1.3	93.3	5.4	0.0	0.55	8.5	35.0	13.1	1.00
21	6.3	67.4	26.3	0.0	0.07	1.0	35.0	1.2	1.00
22	0.6	97.0	2.4	0.0	0.48	7.6	35.0	13.0	1.00
23	0.0	97.6	2.4	0.0	0.47	7.4	35.0	13.0	1.00
24	0.0	97.6	2.4	0.0	0.47	7.4	−160.0	13.0	0.01
25	0.0	97.6	2.4	0.0	0.47	7.4	−162.5	2.0	0.04
26	0.0	99.9	0.1	0.0	0.45	7.2	−162.5	2.0	0.00
27	0.0	48.4	51.6	0.0	0.02	0.2	−162.5	2.0	1.00
28	0.0	48.4	51.6	0.0	0.02	0.2	20.0	2.0	1.00
41	4.8	62.9	32.3	0.0	0.09	1.2	31.6	1.2	1.00
46	13.2	27.4	59.4	0.0	0.16	1.8	40.0	5.0	1.00
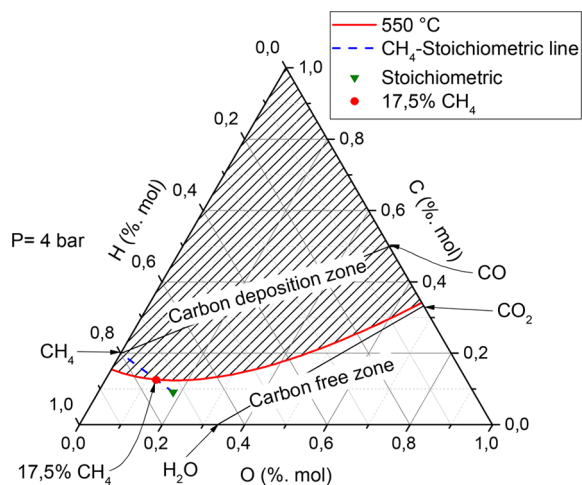
Figure 10. Influence of methane recycle on the methanation feed composition represented on C−H−O ternary diagram.

conditions are also reported on the diagrams: the stoichiometric feed without recycle (0% of CH_4), the full capacity (100% load), and 20% partial load (minimum load) of the plant with recycle. With the plant operating at 100% load the concentration of methane in the methanation reactor feed stream is 1.8%. When the plant is operating at 20% load the worst condition in terms of methane recirculation occurs because the membrane module's active areas are fixed. Therefore, when the plant operates at lower capacity, the flow fed to the membrane modules reduces, resulting in a higher cut ratio. Hence, the relative amount of methane fed to the methanation reactor inlet is higher, reaching its maximum (7.1% CH_4 in the methanation reactor feed) when the plant is operated minimum load. However, in none of the operating conditions has carbon deposition been identified as a

risk. This can be observed on the ternary plots in Figure 11: The operating points fall under the isotherm in the carbon-free zone.

3.3. Heat Integration and Process Efficiency. The electrolyzer heat is not useful because it is generated at low temperature (75−80 °C), and hence no heat recovery is feasible for the plant needs. Because the methanation reaction is highly exothermic, part of the produced heat is used to preheat the methanation feed stream to meet the required temperature at the reactor inlet of 260 °C, while the remaining part is sent to the CO_2 capturing unit. In Figure 12, the Sankey diagram for the energy and mass balance is reported for stationary operation. By using this system integration layout, ∼41% of the heat required by the CO_2 capturing unit is coming from excess heat produced by the methanation reactor.

The overall plant efficiency was evaluated using the general approach suggested by Frank et al.[47] The overall plant efficiency and overall energy utilization factor were calculated with eqs 3 and 4

$$\eta_{0.0.a} = \frac{\dot{E}_{ch,2.2,out}}{\dot{E}_{th,1.4,in} + \dot{Q}_{1.2,in,a} + \dot{Q}_{2.0,in,a} + P_{1.1,a} + P_{2.1,a}} \cdot 100 \tag{3}$$

$$\Theta = \left(1 - \frac{\dot{Q}_{1.0,out} + \dot{Q}_{2.0,out}}{\dot{E}_{th,1.4,in} + \dot{Q}_{1.2,in,a} + \dot{Q}_{2.0,in,a} + P_{1.1,a} + P_{2.1,a}}\right) \cdot 100 \tag{4}$$

where $\dot{E}_{ch,2.2,out}$ is the energy associated with the LNG product stream calculated as the LNG flow rate multiplied by its higher heating value, $\dot{E}_{th,1.4,in} = 0$ is the convective flow of thermal energy associated with the feed of water fed to the electrolyzer, $\dot{Q}_{1.2,in,a} = \dot{Q}_{2.0,in,a} = 0$ is the heat demand by the electrolyzer and methanation units, $P_{1.1,a}$ and $P_{2.1,a}$ are the electricity demand by
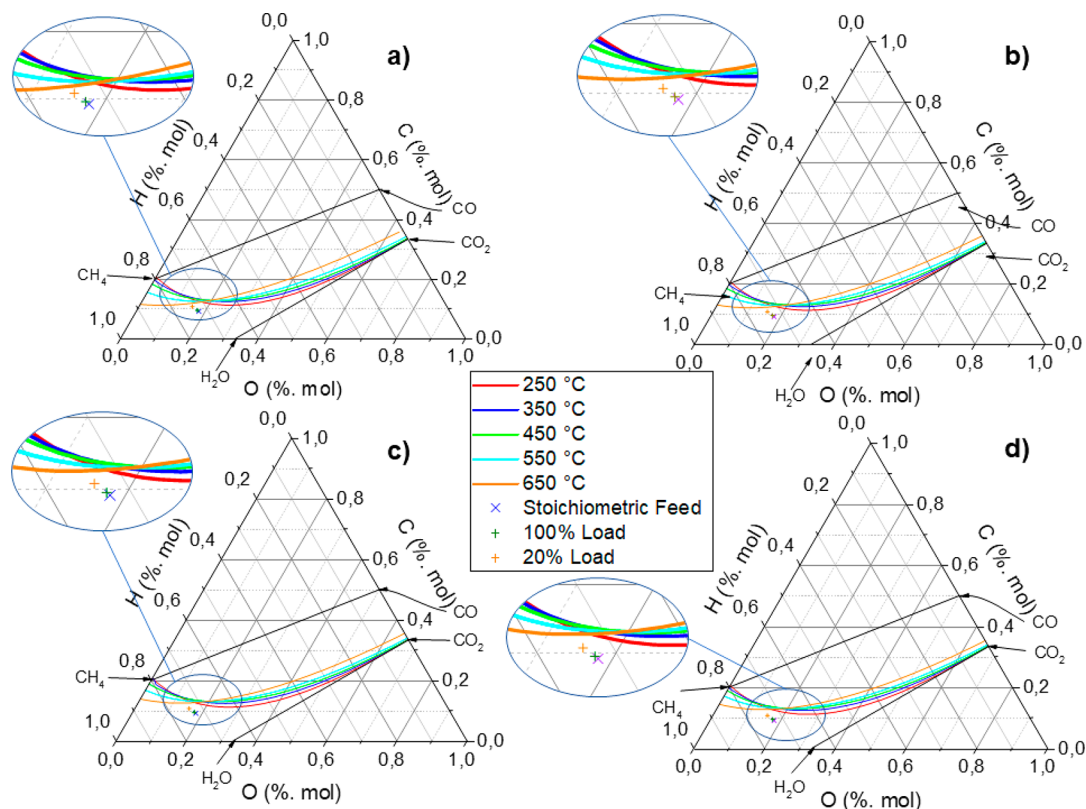
Figure 11. C−H−O ternary diagram at (a) 4, (b) 6, (c) 8, and (d) 10 bar of total pressure.
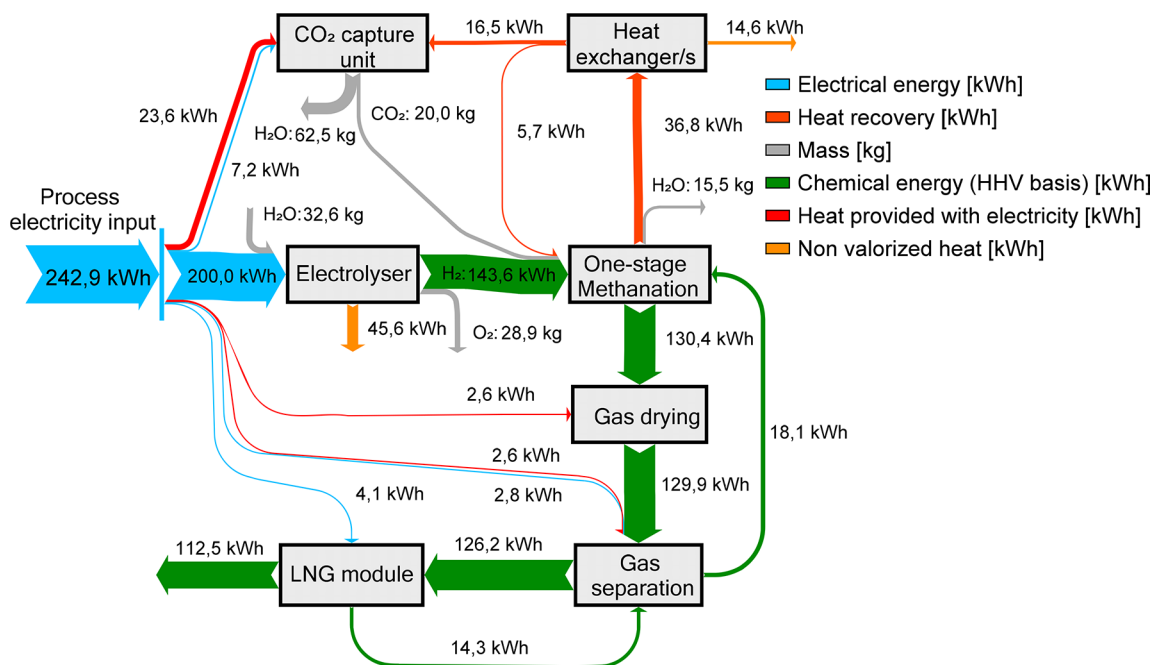

Figure 12. Energy and mass balance Sankey diagram.

the electrolyzer, and the rest of the units, $\dot{Q}_{1.0,out}$ and $\dot{Q}_{2.0,out}$, are usable heat rejected by the electrolyzer and methanation units.

The resulting overall plant efficiency of the demo is $\eta_{0.0.a} = 46.3\%$, and an overall energy utilization factor $\Theta = 75.2\%$, The main loss is due to the electrolyzer module accounting for ∼24% of efficiency reduction.

It is noteworthy that the liquefaction process, a well known energy intensive process, accounts for only 2% relative to the

electrolyzer energy input (or 1.7% of the total energy input). The maximum target energy consumption for this unit is set by design to 1 kWh/kg$_{LNG}$ in alignment with the large-scale plants.[48] Therefore, even in this case the influence on the total energetics of the process would be no more than 3%.

The required energy to inject the produced SNG into the natural gas grid can be evaluated at 1 to 2% of the total energy demand. To liquefy the SNG, the required energy (including the
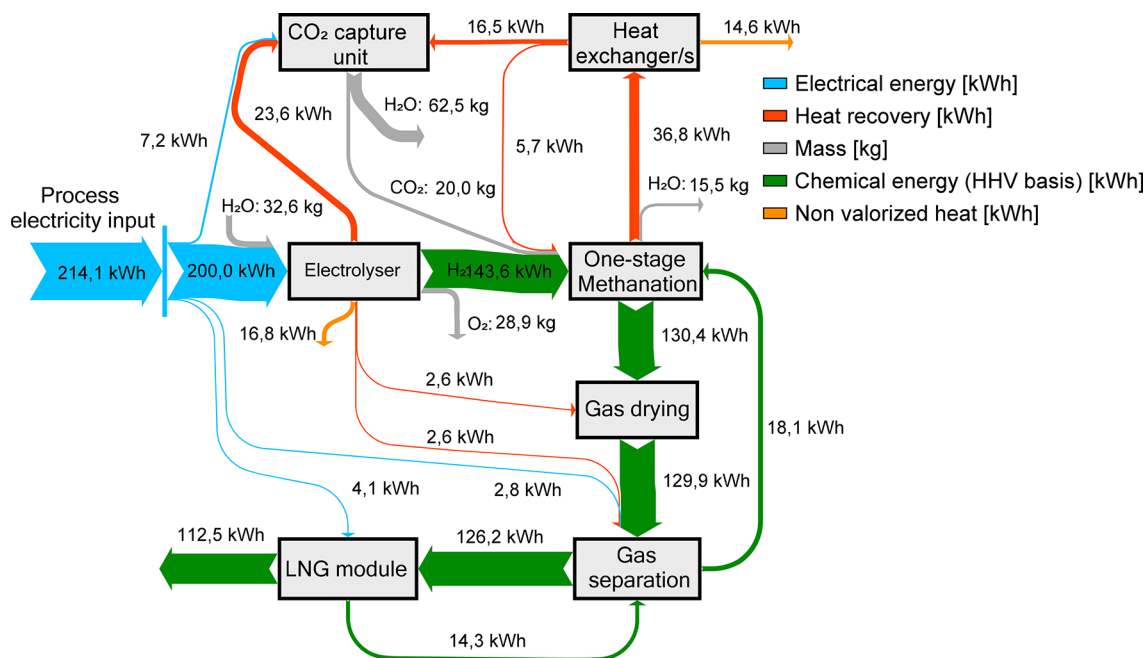
Figure 13. Energy and mass balance Sankey diagram for an improved concept.

liquefaction unit and gas pretreatment) is 4%. Hence, liquefying the product gas has little impact on the plant energetics if compared with grid injection.

Water produced from the methanation unit and CO_2 capturing unit could be used with little to no purification as part of the feed to the electrolyzer, accounting for the total amount of water needed.

3.4. Store&GO Project and Beyond. The power to LNG plant developed in the project could be considered rather complex compared to a more conventional PtG process (e.g., the Audi e-gas plant). However, the increased complexity would be necessary even if the plant ought to produce SNG. In fact, some countries are posing extremely strict limitation on H_2 concentration in the SNG stream to allow injection into the grid (i.e., Italy being one of them <0.5% of H_2). Figures 3−5 show that to not to exceed a H_2 content of 0.5%, none of those supposed simpler configurations is possible. Therefore, a separation system with gas recycle, coupled to a strong simplification of employing only one reactor (instead of a minimum of two reactors as in conventional architectures; see Figure 5), makes the current plant not more complex than other solutions. Moreover, the separation and recycle system allows us to cope with the eventual fluctuations of the H_2 and CO_2 feeds, which might not be instantaneously in stoichiometric ratio. Finally, LNG is not an added complexity but just a business opportunity. In fact, with a small tuning of the membrane modules, the plant could also work just to produce SNG. The gas could then be injected in the gas grid with the strictest specification of hydrogen concentration today in Europe.

The power to gas plants are expected to also work in transient operation, following the renewable electricity production and providing grid balancing. Therefore, different electricity input profiles will be used to stress test the entire demo system as well as cold and hot standby start-up times. This will be one of the outcomes of the Store&GO project. The objective is to have a plant that can work in transient operation and use the buffers only for balance of plant purposes (i.e., different electrolyzer and methanation dynamics).

One limiting factor in the application of PtG technologies is the electrolysis. As previously mentioned, the most mature and cost-effective (in terms of investment and maintenance cost per kilowatt installed) is the AEC. In general, commercially available AEC units operate at temperature below 100 °C, but also higher temperatures are being studied.[49−51] An electrolyzer able to operate at temperatures >140 °C would allow us to recover and use the generated heat in the CO_2 capture unit and the two TSA units, ideally covering their entire heat requirement (46.5 kWh produced by the electrolyzer vs 46.3 kWh of heat required by the units). If this electrolyzer would have the same electric to H_2 efficiency as the one used in the demo plant, then the process efficiency would increase to 52.6% and the overall energy utilization would increase to 85.3%.

Moreover, a higher working temperature electrolyzer module would likely lead to an increase in electrolyzer efficiency (i.e., electrolyte ohmic resistance reduction and reaction kinetics improve with temperature increase[52,53]), thus leading to an even higher increase in the plant efficiency. In Figure 13, the revised Sankey diagram with the new improved concept is reported.

The efficiency attainable with the improved concept is similar to that of other PtG plants. The Audi e-gas project is the best example because it uses basically the same electrolysis technology (alkaline electrolyzer). The efficiency reported in this case is 54 ± 3% before heat integration with the neighboring biogas plant[22] versus 52.6% of this concept.

4. CONCLUSIONS

A concept to produce synthetic LNG using hydrogen generated from excess renewable electricity and carbon dioxide captured from air was analyzed in this study. Process simulations of the concept were performed including optimization of single units and whole plant by including thermal integration. The simulation model accounted for the efficiency of commercially available technologies (i.e., electrolysis and CO_2 capture).

A thermodynamic analysis focused on the methanation reactor excluded the carbon formation in the range of possible operating conditions. Subsequently, a membrane gas separation

system was developed: screening of different membranes and choosing the appropriate module layout. A two-stage membrane system was adequate for the stream purification. Besides this, choosing the appropriate separation system would give the possibility for the produced gas to be injected into the natural gas grid or undergo liquefaction, allowing for a flexible operation. Afterward, the optimization of the SMR liquefaction system confirmed that the tested refrigerant compositions can be used. Among the several considered mixtures, the ethylene–propane refrigerant gave the lowest energy consumption of 0.57 kWh/kg_{LNG}.

Finally, after heat recovery, an overall plant efficiency of 46.3% electrical to chemical conversion was calculated for the demo plant. However, the use of an electrolysis system operating temperatures higher than 140 °C would allow us to recover the produced heat and use it in the carbon-dioxide-capturing unit and the two TSA modules. This would allow us to reach an electrical to chemical efficiency of 52.6%.

■ AUTHOR INFORMATION

Corresponding Author
*E-mail: samir.bensaid@polito.it.

ORCID ⊙
Samir Bensaid: 0000-0001-9634-266X

Notes
The authors declare no competing financial interest.

■ ACKNOWLEDGMENTS

■ ABBREVIATIONS

LNG = liquefied natural gas
RES = renewable energy source
SMR = single mixed refrigerant
PtG = power to gas
IPCC = International Panel on Climate Change
EU = European Union
SNG = substitute natural gas
CNG = compressed natural gas
L-CNG = liquefied-compressed natural gas
AEC = alkaline electrolysis cell
PEMEC = polymeric electrolyte membrane electrolysis cell
SOEC = solid oxide electrolysis cell
LHV = lower heating value
HHV = higher heating value
ΔH_{298K} = specific heat of reaction at 298 K = BOG = boil-off gas
TSA = temperature swing adsorption
AC = Alternated current
$\dot{n}$ = molar flow rate

■ REFERENCES

(1) Pachauri, R. K.; Allen, M. R.; Barros, V. R.; Broome, J.; Cramer, W.; Christ, R. *Climate Change 2014 Synthesis Report*; IPCC: Geneva, Switzerland, 2014.

(2) Zervos, A.; Lins, C.; Tesnière, L. *Mapping Renewable Energy Pathways towards 2020: EU Roadmap*; European Renewable Energy Council: Brussels, 2011.

(3) Akinyele, D. O.; Rayudu, R. K. Review of Energy Storage Technologies for Sustainable Power Networks. *Sustain. Energy Technol. Assessments* **2014**, *8*, 74−91.

(4) Divya, K. C.; Østergaard, J. Battery Energy Storage Technology for Power Systems-An Overview. *Electr. Power Syst. Res.* **2009**, *79* (4), 511−520.

(5) Lund, H.; Salgi, G. The Role of Compressed Air Energy Storage (CAES) in Future Sustainable Energy Systems. *Energy Convers. Manage.* **2009**, *50* (5), 1172−1179.

(6) Deane, J. P.; Ó Gallachóir, B. P.; McKeogh, E. J. Techno-Economic Review of Existing and New Pumped Hydro Energy Storage Plant. *Renewable Sustainable Energy Rev.* **2010**, *14* (4), 1293−1302.

(7) Götz, M.; Lefebvre, J.; Mörs, F.; McDaniel Koch, A.; Graf, F.; Bajohr, S.; Reimert, R.; Kolb, T. Renewable Power-to-Gas: A Technological and Economic Review. *Renewable Energy* **2016**, *85*, 1371−1390.

(8) Meiri, N.; Radus, R.; Herskowitz, M. Simulation of Novel Process of CO_2 Conversion to Liquid Fuels. *J. CO₂ Util.* **2017**, *17*, 284−289.

(9) Chen, H.; Cong, T. N.; Yang, W.; Tan, C.; Li, Y.; Ding, Y. Progress in Electrical Energy Storage System: A Critical Review. *Prog. Nat. Sci.* **2009**, *19* (3), 291−312.

(10) Castillo, A.; Gayme, D. F. Grid-Scale Energy Storage Applications in Renewable Energy Integration: A Survey. *Energy Convers. Manage.* **2014**, *87*, 885−894.

(11) Ibrahim, H.; Ilinca, A.; Perron, J. Energy Storage Systems—Characteristics and Comparisons. *Renewable Sustainable Energy Rev.* **2008**, *12* (5), 1221−1250.

(12) Luo, X.; Wang, J.; Dooner, M.; Clarke, J. Overview of Current Development in Electrical Energy Storage Technologies and the Application Potential in Power System Operation. *Appl. Energy* **2015**, *137*, 511−536.

(13) Hashimoto, K.; Yamasaki, M.; Fujimura, K.; Matsui, T.; Izumiya, K.; Komori, M.; El-Moneim, A.; Akiyama, E.; Habazaki, H.; Kumagai, N.; et al. Global CO_2 Recycling—novel Materials and Prospect for Prevention of Global Warming and Abundant Energy Supply. *Mater. Sci. Eng., A* **1999**, *267* (2), 200−206.

(14) Hashimoto, K.; Kumagai, N.; Izumiya, K.; Takano, H.; Kato, Z. The Production of Renewable Energy in the Form of Methane Using Electrolytic Hydrogen Generation. *Energy. Sustain. Soc.* **2014**, *4* (1), 17.

(15) Choi, S.; Gray, M. L.; Jones, C. W. Amine-Tethered Solid Adsorbents Coupling High Adsorption Capacity and Regenerability for CO_2 Capture From Ambient Air. *ChemSusChem* **2011**, *4* (5), 628−635.

(16) NGVA Europe. *NGVA Europe*. https://www.ngva.eu/ (accessed April 3, 2017).

(17) LNG Blue Corridors Consortium. *LNG Blue Corridors*. http://lngbc.eu/ (accessed April 3, 2017).

(18) *Enabling Clean Marine Transport*; International Gas Union: Barcelona, Spain, 2017.

(19) Burel, F.; Taccani, R.; Zuliani, N. Improving Sustainability of Maritime Transport through Utilization of Liquefied Natural Gas (LNG) for Propulsion. *Energy* **2013**, *57*, 412−420.

(20) Kumar, S.; Kwon, H. T.; Choi, K. H.; Lim, W.; Cho, J. H.; Tak, K.; Moon, I. LNG: An Eco-Friendly Cryogenic Fuel for Sustainable Development. *Appl. Energy* **2011**, *88* (12), 4264−4273.

(21) German Energy Agency (dena). *The Power to Gas Strategy Platform*. http://www.powertogas.info/power-to-gas/pilotprojekte-im-ueberblick/audi-e-gas-projekt/ (accessed January 8, 2018).

(22) Bailera, M.; Lisbona, P.; Romeo, L. M.; Espatolero, S. Power to Gas Projects Review: Lab, Pilot and Demo Plants for Storing Renewable Energy and CO_2. *Renewable Sustainable Energy Rev.* **2017**, *69*, 292−312.

(23) HelmetH Consortium. *HELMETH Project*. http://www.helmeth.eu/ (accessed January 8, 2018).

(24) Store&GO Consortium. *Store&GO*. http://www.storeandgo.info/ (accessed March 31, 2017).

(25) INGRID consortium. *INGRID-High-Capacity Hydrogen-Based Green-Energy Storage Solutions for Grid Balancing*. http://www.ingridproject.eu/ (accessed December 4, 2017).

(26) Holladay, J. D.; Hu, J.; King, D. L.; Wang, Y. An Overview of Hydrogen Production Technologies. *Catal. Today* **2009**, *139* (4), 244−260.

(27) Ramdin, M.; De Loos, T. W.; Vlugt, T. J. H. State-of-the-Art of CO_2 Capture with Ionic Liquids. *Ind. Eng. Chem. Res.* **2012**, *51* (24), 8149−8177.

(28) Wang, T.; Hou, C.; Ge, K.; Lackner, K. S.; Shi, X.; Liu, J.; Fang, M.; Luo, Z. Spontaneous Cooling Absorption of CO_2 by a Polymeric Ionic Liquid for Direct Air Capture. *J. Phys. Chem. Lett.* **2017**, *8* (17), 3986−3990.

(29) Wang, Y.; Du, T.; Song, Y.; Che, S.; Fang, X.; Zhou, L. Amine-Functionalized Mesoporous ZSM-5 Zeolite Adsorbents for Carbon Dioxide Capture. *Solid State Sci.* **2017**, *73*, 27−35.

(30) Chen, X. Y.; Vinh-Thang, H.; Rodrigue, D.; Kaliaguine, S. Amine-Functionalized MIL-53 Metal−Organic Framework in Polyimide Mixed Matrix Membranes for CO_2/CH_4 Separation. *Ind. Eng. Chem. Res.* **2012**, *51* (19), 6895−6906.

(31) Wang, X.; Guo, Q.; Zhao, J.; Chen, L. Mixed Amine-Modified MCM-41 Sorbents for CO_2 Capture. *Int. J. Greenhouse Gas Control* **2015**, *37*, 90−98.

(32) Chaffee, A. L.; Knowles, G. P.; Liang, Z.; Zhang, J.; Xiao, P.; Webley, P. A. CO_2 Capture by Adsorption: Materials and Process Development. *Int. J. Greenhouse Gas Control* **2007**, *1* (1), 11−18.

(33) Climeworks. *Climeworks*. http://www.climeworks.com/ (accessed May 23, 2017).

(34) Tevebaugh, A. D.; Cairns, E. J. Carbon Deposition Boundaries in the CHO System at Several Pressures. *J. Chem. Eng. Data* **1965**, *10* (4), 359−362.

(35) Frick, V.; Brellochs, J.; Specht, M. Application of Ternary Diagrams in the Design of Methanation Systems. *Fuel Process. Technol.* **2014**, *118*, 156−160.

(36) National Institute of Standards and Technology (NIST). *NIST Chemistry WebBook*; NIST: Gaithersburg, MD. http://webbook.nist.gov/ (accessed January 20, 2017).

(37) Scholz, M.; Melin, T.; Wessling, M. Transforming Biogas into Biomethane Using Membrane Technology. *Renewable Sustainable Energy Rev.* **2013**, *17*, 199−212.

(38) Scholes, C. A.; Stevens, G. W.; Kentish, S. E. Membrane Gas Separation Applications in Natural Gas Processing. *Fuel* **2012**, *96*, 15−28.

(39) Pettersen, T.; Lien, K. M. A New Robust Design Model for Gas Separating Membrane Modules, Based on Analogy with Counter-Current Heat Exchangers. *Comput. Chem. Eng.* **1994**, *18* (5), 427−439.

(40) Lim, W.; Choi, K.; Moon, I. Current Status and Perspectives of Liquefied Natural Gas (LNG) Plant Design. *Ind. Eng. Chem. Res.* **2013**, *52* (9), 3065−3088.

(41) Remeljej, C. W.; Hoadley, A. F. A. An Exergy Analysis of Small-Scale Liquefied Natural Gas (LNG) Liquefaction Processes. *Energy* **2006**, *31* (12), 2005−2019.

(42) Austbø, B.; Løvseth, S. W.; Gundersen, T. Annotated Bibliography—Use of Optimization in LNG Process Design and Operation. *Comput. Chem. Eng.* **2014**, *71*, 391−414.

(43) Cao, L.; Liu, J.; Xu, X. Robustness Analysis of the Mixed Refrigerant Composition Employed in the Single Mixed Refrigerant (SMR) Liquefied Natural Gas (LNG) Process. *Appl. Therm. Eng.* **2016**, *93*, 1155−1163.

(44) Xu, X.; Liu, J.; Cao, L. Optimization and Analysis of Mixed Refrigerant Composition for the PRICO Natural Gas Liquefaction Process. *Cryogenics* **2014**, *59*, 60−69.

(45) Adewole, J. K.; Ahmad, A. L.; Ismail, S.; Leo, C. P. Current Challenges in Membrane Separation of CO2 from Natural Gas: A Review. *Int. J. Greenhouse Gas Control* **2013**, *17*, 46−65.

(46) Union Gas Limited. *Union Gas*. https://www.uniongas.com/about-us/about-natural-gas/chemical-composition-of-natural-gas (accessed June 19, 2018).

(47) Frank, E.; Gorre, J.; Ruoss, F.; Friedl, M. J. Calculation and Analysis of Efficiencies and Annual Performances of Power-to-Gas Systems. *Appl. Energy* **2018**, *218*, 217−231.

(48) The Linde Group. *StarLNGL*. https://www.linde-engineering.com/en/process_plants/lng-and-natural-gas-processing-plants/liquefied_natural_gas/starlngl/index.html (accessed June 19, 2018).

(49) Gahleitner, G. Hydrogen from Renewable Electricity: An International Review of Power-to-Gas Pilot Plants for Stationary Applications. *Int. J. Hydrogen Energy* **2013**, *38* (5), 2039−2061.

(50) Ganley, J. C. High Temperature and Pressure Alkaline Electrolysis. *Int. J. Hydrogen Energy* **2009**, *34* (9), 3604−3611.

(51) Allebrod, F.; Chatzichristodoulou, C.; Mogensen, M. B. Alkaline Electrolysis Cell at High Temperature and Pressure of 250 °C and 42 bar. *J. Power Sources* **2013**, *229*, 22−31.

(52) Buttler, A.; Spliethoff, H. Current Status of Water Electrolysis for Energy Storage, Grid Balancing and Sector Coupling via Power-to-Gas and Power-to-Liquids: A Review. *Renewable Sustainable Energy Rev.* **2018**, *82* (3), 2440−2454.

(53) Ursua, A.; Gandia, L. M.; Sanchis, P. Hydrogen Production From Water Electrolysis: Current Status and Future Trends. *Proc. IEEE* **2012**, *100* (2), 410−426.

(54) Gassner, M.; Baciocchi, R.; Maréchal, F.; Mazzotti, M. Integrated Design of a Gas Separation System for the Upgrade of Crude SNG with Membranes. *Chem. Eng. Process.* **2009**, *48* (9), 1391−1404.

(55) Wang, Z.; Wang, D.; Zhang, F.; Jin, J. Tröger's Base-Based Microporous Polyimide Membranes for High-Performance Gas Separation. *ACS Macro Lett.* **2014**, *3* (7), 597−601.

(56) Lin, W.-H.; Chung, T.-S. Gas Permeability, Diffusivity, Solubility, and Aging Characteristics of 6FDA-Durene Polyimide Membranes. *J. Membr. Sci.* **2001**, *186* (2), 183−193.

(57) Han, S. H.; Lee, J. E.; Lee, K. J.; Park, H. B.; Lee, Y. M. Highly Gas Permeable and Microporous Polybenzimidazole Membrane by Thermal Rearrangement. *J. Membr. Sci.* **2010**, *357* (1−2), 143−151.